TM-71-2015-4

TECHNICAL MEMORANDUM

DENSITY AND FLUX DISTRIBUTIONS OF NEUTRAL GASES IN THE LUNAR ATMOSPHERE - CASE 340

Bellcomm

BELLCOMM, INC.
955 L'ENFANT PLAZA NORTH, S.W. WASHINGTON, D.C. 20024

COVER SHEET FOR TECHNICAL MEMORANDUM

TITLE- Density and Flux Distributions of Neutral Gases in the Lunar Atmosphere

TM- 71-2015-4

DATE- June 24, 1971

FILING CASE NO(S)- 340

AUTHOR(S)- T. T. J. Yeh
G. K. Chang

FILING SUBJECT(S)-
(ASSIGNED BY AUTHOR(S)- Lunar Atmosphere

ABSTRACT

Using the kinetic theory of gases, we have calculated numerically the density and flux distributions in the lunar atmosphere due to gas temperature and density variations at the surface, which are assumed known. Computation of neon density distributions along a 100 km equatorial circular orbit shows that the density on the day side is about one order of magnitude higher than that on the night side in the case of a uniform surface gas density N_o (case 1), but is a factor of 2 smaller in the case of $N_o \sim T_o^{-5/2}$ (case 2), as given by Hodges and Johnson, where T_o is the gas temperature at the surface. For argon, the corresponding values for these two cases are $\sim 2.5 \times 10^2$ and 10. Density profiles generally have smooth transitions near the terminator, but a peak occurs for neon in case 2. In the 8 x 60 nm elliptic descent orbit of Apollo 15, the relative changes of density in the above two cases are ~ 50 and ~ 25

for neon, and $\sim 3 \times 10^3$ and $\sim 7 \times 10^2$ for argon; at the sunrise terminator, density distributions for both neon and argon are sharply peaked in case 2. Computation of flux distributions versus altitude over the equatorial terminator shows that a positive net flux from the hot side to the cold side persists at all altitudes in case 1; however, in case 2, the net flux is positive at higher altitudes but negative at lower altitudes. The density distribution of hydrogen in the 100 km orbit derived from the surface flux distribution given by Vogel indicates substantial lateral transport as well as particle loss due to thermal escape.

Comparison of the theoretical results derived here with Apollo Orbital Mass Spectrometer Experiment data should enable discrimination between various models of gas density variations over the lunar surface. Once the latter variations will be measured, comparison of surface and orbital experimental data with the theoretical results will shed clear light on the dynamic processes shaping the lunar atmosphere.

Bellcomm

955 L'Enfant Plaza North, S.W.
Washington, D. C. 20024

TM-71-2015-4

date: June 24, 1971

to: Distribution

from: T. T. J. Yeh, G. K. Chang

subject: Density and Flux Distributions of Neutral Gases in the Lunar Atmosphere - Case 340

TECHNICAL MEMORANDUM

Introduction

The lunar atmosphere has long been known to be extremely tenuous. Pre-Apollo estimates of particle concentration at the lunar surface, including possible sources and various removal processes, were recently reviewed by Groves (1967) and Johnson (1971). Particle concentrations of neutral gases at the surface were generally considered to lie in the range of 10^5 to 10^6 cm^{-3}. Preliminary results from the Apollo 14 Cold Cathode Gage Experiment (CCGE) (Johnson et al., 1971) have confirmed these values for the first time by direct measurements. However, since the lunar surface temperature exhibits strong variation and the atmospheric density at the surface may vary as well, lateral transport of gases through the lunar atmosphere has drawn considerable interest.

Hodges and Johnson (1968) made a study on the lateral transport of neutral gases in an exosphere, including the effect of planetary rotations. On assuming local zero

net flux at the surface, they show that in the absence of significant sources and sinks, the atmospheric surface temperature and concentration tend to obey $N_o T_o^{5/2}$ = constant if there is no rotation, and $N_o T_o$ = constant if rotational effects dominate; here N_o and T_o are the gas density and temperature at the surface. The velocity of the lunar surface due to rotation is considerably smaller than the average thermal velocity of gases of interest, such as neon and argon, and we, therefore, neglect the rotational effect in the present study. Vogel (1966) investigated the molecular fluxes, in a steady state case, at the base of the lunar atmosphere. He showed that if any loss mechanisms for the gas particles exist, there must be a steady source of gas in order to maintain a steady state flux distribution. The thermal escape is the predominant loss mechanism for light gases, such as hydrogen and helium. For heavier gases the lifetime against thermal escape is long; they are swept out of the lunar atmosphere by the solar wind following photo-ionization and charge exchange. However, the time scale of these processes is on the order of 10^7 seconds (Johnson, 1971), which is considerably larger than the transport time, which is at most on the order of 10^4 seconds (Grove, 1967). Hence, we also neglect the ionization loss during flight of these gas particles.

The studies of both Hodges and Johnson (1968) and of Vogel (1966) were restricted to the density or flux distributions at the surface, i.e., a two-dimensional problem. On the other hand, the orbital and surface mass spectrometer experiments of the Apollo 15, 16 and 17 missions are designed to measure the density and flux distributions above the surface as well as on it. A new analysis in support of the experiments is therefore desirable. The information obtained from these measurements and analysis will greatly improve the understanding of the gas transport process in the lunar atmosphere. Furthermore, the results of Hodges and Johnson (1968) and of Vogel (1966) are model dependent. By comparing the orbital mass spectrometer measurements with the theoretical analysis it may be possible to discriminate between the various models for the surface density and flux distributions.

Consequently, in the present investigation, we extend the calculations of density and flux distributions to the three-dimensional case, i.e., the region of interest is the entire space above the lunar surface. Our approach is unique in that the density and flux (and any other macroscopic physical quantities) are treated under the same framework. It follows from the kinetic theory of gases that, once the distribution function is known, the density and fluxes may be obtained by taking the moments of the distribution function. For the case of neutral particles in an exosphere, as is the

case of the lunar atmosphere, the calculation is straightforward. The above calculations, however, require the surface density or flux as the boundary condition. Several surface density and flux distributions, including those of Hodges and Johnson (1968) and Vogel (1966), are used in the present investigation so that such parametric studies may be compared with actual measurements.

Gas Transport Model

The model adopted for the study of neutral gas transport is an exosphere whose base is the surface of a perfectly spherical moon. All of the gas particles are originating from (or underneath) the surface and travel with free trajectories through the exosphere under the lunar gravitational force until they land on the surface or escape to the space. In other words, collisions between gas particles are neglected. This also implies that non-thermal escape mechanisms such as photo-ionization and removal by the solar wind are regarded as secondary effects. We also assume a steady state situation. Furthermore, when a particle lands on the lunar surface, we shall assume that it is adsorbed by the surface, thermalized and then re-emitted according to the local surface conditions. This is equivalent to the diffusive reflection condition with thermal energy changes. In a steady state situation, we shall not distinguish between the originally emitted and re-emitted particles, except when volcanic sources

are considered. For simplicity, the angular velocity of the moon is neglected. These assumptions are similar to those of Vogel (1966) and Hodges and Johnson (1968), except that the latter investigators included the rotational effect.

In the present model, if a particle originates from the surface, where the coordinate is $\underline{x}_o$ and the velocity vector is $\underline{v}_o$, its position $\underline{x}$ and velocity $\underline{v}$ at a later time can be calculated from the trajectory equations. Conversely, if an observer located at a position $\underline{x}$ in space sees a particle having a velocity vector $\underline{v}$, he can, by following the particle's trajectory, always trace back its initial position $\underline{x}_o$ and velocity $\underline{v}_o$ at the surface (see Figure 1). By summing over all possible velocities, an observer at $\underline{x}$ counts all the particles originating from the entire lunar surface that reach $\underline{x}$. If a statistical analysis with appropriate weighting is performed, the density and fluxes can be easily obtained. In this model, particles with all possible energies, including those exceeding the escaping energy, are accounted for. The detailed formulation based on the kinetic theory of gases is given below.

Basic Kinetic Equation

We shall describe the neutral particles (molecules, atoms) by the distribution function

$$f(\underline{x}, \underline{v}, t)$$

which is defined as follows. The product of f with the volume element in phase space ($\underline{x}$, $\underline{v}$), i.e.,

$$f(\underline{x}, \underline{v}, t)\ d^3x\ d^3v,$$

is the number of particles whose coordinates at time t lie between $\underline{x}$ and $\underline{x} + d\underline{x}$, and whose velocities are between $\underline{v}$ and $\underline{v} + d\underline{v}$. The particle density and other average quantities can be expressed in terms of the function f. For instance, the density is

$$n(\underline{x}, t) = \int f(\underline{x}, \underline{v}, t)\ d^3v, \tag{1}$$

and the particle flux in the i-direction is

$$\underline{\psi}_i(\underline{x},t) = \int \underline{v}_i\ f(\underline{x}, \underline{v}, t) d^3v \tag{2}$$

where $\underline{v}_i$ is the velocity along the directior i. In general there will be a distribution function for each species of gas. In such a case, a subscript j may be attached to f to indicate that particular species.

As is well known, the distribution function obeys the Boltzmann equation. In the absence of collisions, it is of the following form:

$$\frac{\partial f}{\partial t} + \underline{v} \cdot \nabla f + \underline{F} \cdot \nabla_v f = 0 \tag{3}$$

where $\underline{F}$ is the force per unit mass acting on a particle, and ∇ and ∇_v are respectively the gradient operators in position and velocity space.

We shall choose a spherical polar coordinate system fixed on the moon such that r is the radial distance measured from the center of the moon, θ is the co-latitude measured from the north pole, and ϕ is the longitude measured from the subsolar point. The force field $\underline{F}$ in the present problem is the gravitational force which is equal to $-\mu/r^2$, where μ is the lunar gravitational constant (universal gravitational constant times the mass of the moon). The explicit expression of the kinetic equation in the spherical polar coordinates is given in Appendix A.

The general solution of Eq. 3, which is well known, is that f is any arbitrary function of the integrals of the Lagrangian subsidiary equations

$$\frac{d\underline{x}}{dt} = \underline{v}, \qquad \frac{d\underline{v}}{dt} = \underline{F}. \tag{4}$$

Eqs. (4) are just the equations of motion of the particle under the force field $\underline{F}$. The explicit form of Eqs. (4) in spherical coordinates is also given in Appendix A. These equations are also referred to as the trajectory equations in phase space. In fact, the statement for the general solution of f means that f is a constant in time along a trajectory in phase space. In other words, if f is known at one time, the

value of f is conserved for all times along a trajectory in phase space. The particular value of f at ($\underline{x}$, $\underline{v}$, t) is, therefore, determined by the particular trajectories in question and the initial distribution functions at the boundary $f(\underline{x}_o, \underline{v}_o, 0)$. Consequently, $f(\underline{x}, \underline{v}, t)$ may be expressed by the following relation:

$$f(\underline{x}, \underline{v}, t) = \int f(\underline{x}_o, \underline{v}_o, 0)\ \delta(\underline{x}-\underline{X})\delta(\underline{v}-\underline{V})\ d^3x_o d^3v_o \qquad (5)$$

where

$$\underline{x} = \underline{X}\ (\underline{x}_o, \underline{v}_o, t)$$

and (6)

$$\underline{v} = \underline{V}\ (\underline{x}_o, \underline{v}_o, t)$$

are the position and velocity trajectories of a single particle parameterized in terms of its initial conditions $\underline{x}_o$ and $\underline{v}_o$ as well as the time. That is, Eqs. (6) are the solution of Eqs. (4). In a steady state case $f = f(\underline{x},\underline{v})$, the time t may be considered as a free parameter in Eqs. (6). This method of determining $f(\underline{x}, \underline{v}, t)$ by tracing it back to its initial and boundary conditions along each individual particle trajectory is referred to as the method of characteristics, since, in mathematical terminology, Eqs. (4) are also the characteristic equations of the partial differential equation (1). In this method, it is essential to determine the particle's trajectory, or the characteristics of the system, i.e., the solution of Eqs. (4). This is done in the next section.

Particle Trajectories in Fixed Spherical Coordinates

Usually, the particle trajectories can be obtained by direct integration of Eqs. (4). However, since Eqs. (4) are a set of coupled equations (see Appendix A), we shall determine the trajectories via a different approach - by means of Hamilton-Jacobi Theory* (e.g., Goldstein, 1953). The detailed derivation of the particle trajectories is given in Appendix B. The results are as follows:

$$\frac{1}{2}(v_r^2 + v_\theta^2 + v_\phi^2) - \frac{\mu}{r} = \frac{1}{2}(v_{r_o}^2 + v_{\theta_o}^2 + v_{\phi_o}^2) - \frac{\mu}{r_o} \tag{7}$$

$$r \sin\theta\, v_\phi = r_o \sin\theta_o\, v_{\phi_o} \tag{8}$$

$$r^2(v_\theta^2 + v_\phi^2) = r_o^2(v_{\theta_o}^2 + v_{\phi_o}^2) \tag{9}$$

$$\cos^{-1}\left(\cos\theta \Big/ \sqrt{1 - \frac{v_\phi^2 \sin^2\theta}{v_\theta^2 + v_\phi^2}}\right) \pm \cos^{-1}\left[\left(1 - \frac{r(v_\theta^2 + v_\phi^2)}{\mu}\right)/\varepsilon\right]$$

$$= \cos^{-1}\left(\cos\theta_o \Big/ \sqrt{1 - \frac{v_\phi^2 \sin^2\theta}{v_\theta^2 + v_\phi^2}}\right) + \cos^{-1}\left[\left(1 - \frac{r^2(v_\theta^2 + v_\phi^2)}{r_o \mu}\right)/\varepsilon\right] \tag{10}$$

*A different method may be used. For a two-body central force problem, the particle's motion is always in a plane. The trajectory may be elliptic, parabolic or hyperbolic depending on particular parameters (so called orbit elements) which determine the trajectory. That particular plane, and the particle's motion on that plane, may then be transformed to the fixed reference coordinates (r,θ,ϕ). However, since particles may emerge from every location on the lunar surface, and may have all possible velocities, such transformation becomes rather cumbersome and the application of Hamilton-Jacobi Theory is more convenient.

where

$$\varepsilon = [1 + \frac{r^2}{\mu^2}(v_r^2 + v_\theta^2 + v_\phi^2 - \frac{2\mu}{r})(v_\theta^2 + v_\phi^2)]^{1/2} \qquad (10a)$$

$$\phi - \phi_o = -\tan^{-1}\left(\frac{v_\phi \cos\theta}{v_\theta}\right) + \tan^{-1}\left(\frac{v_\phi \sin\theta \cos\theta_o}{\sqrt{(v_\theta^2+v_\phi^2)\sin^2\theta_o - v_\phi^2 \sin^2\theta}}\right) \qquad (11)$$

In the above equations, r_o, θ_o, ϕ_o are the coordinates of the lunar surface where gas particles are emitted with velocity components V_{r_o}, V_{θ_o}, and V_{ϕ_o}. Eqs. (7) - (9) give respectively the total energy, ϕ-component angular momentum, and total angular momentum squared per unit mass of a particle, which are constants of the motion for a particular trajectory. Eqs. (10) and (11) describe the trajectory in position space. The time of flight of the particle is eliminated from Eqs. (7) - (11) in such a way that the initial time $t = 0$ is taken at the instant when the particle leaves the lunar surface at a position (r_o, θ_o, ϕ_o). The signs on the second term of Eq. (10) is taken according to the sign of v_r.

Boundary Condition of f

In order to complete the formulation of the problem, the boundary condition of f must be given. In the present model, we need only prescribe f for the particles emitted at the lunar surface. For simplicity, we shall assume that f is Maxwellian at the surface characterized by the local surface temperature. The same distribution function was also

used by previous investigators (Hodges and Johnson, 1968, Vogel, 1966). It should be remarked, however, that other types of distribution functions may also be chosen. For instance, if the gas comes from some distance below the surface, the temperature there may be different from that at the surface; or if there are volcanic sources, the distribution function may be close to localized delta functions. Furthermore, it should be noted that although f is locally Maxwellian at the surface, it is not in equilibrium in space above the surface. This is due to lack of a collisional mechanism to equilibrate the gas particles. The escape mechanism also tends to destroy the equilibrium.

For a Maxwellian distribution at the surface, f may be written as:

$$f(\underline{x}_o, \underline{v}_o) = N_o(\underline{x}_o)\,[m/2\pi kT_o(\underline{x}_o)]^{3/2} \exp\,[-m\underline{v}_o^{\,2}/2kT_o(\underline{x}_o)], \qquad (12)$$

where

$$\underline{v}_o^{\,2} = v_{r_o}^{\,2} + v_{\theta_o}^{\,2} + v_{\phi_o}^{\,2} \quad . \qquad (13)$$

In the above equations, T_o is the temperature at the surface, N_o is twice the concentration of emitted particles at the surface; both T_o and N_o are functions of the lunar surface coordinates $\underline{x}_o$ (r_o = lunar radius, θ_o, ϕ_o), m is the mass of the particle, and k is the Boltzmann constant.

Lunar Surface Temperature Variation

The temperature of the lunar surface may be, in principle, determined by the balance of heat fluxes of incident solar radiation, reflected and emitted radiations and thermal conduction. The variation of the surface temperature of a point on the lunar equator during a complete lunation may be represented by the plot shown in Figure 2 (NEPSAP, 1969). The noon-time temperature is ∿385°K, decreasing approximately as the cosine of the solar angle to the 1/4 - 1/6 power. The night-time temperature is ∿100°K with relatively small variations. Note that the temperature after sunset is somewhat higher than that before sunrise because of thermal inertia. For a point at some higher latitude, the temperature decreases approximately as the cosine of the latitude to the 1/4 power, as compared with the temperature of an equatorial point at the same longitude (NEPSAP, 1969). This relation may be written as:

$$T_o(\theta_o, \phi_o) = T_{eq}(\phi_o)\sin^{1/4}\theta_o \qquad (14)$$

where θ_o is the colatitude measured from the north pole and ϕ_o is the longitude measured from the subsolar point. T_{eq} is the temperature at the equator and is given in Figure 2. However, for computational purpose, we shall idealize the temperature profile of T_{eq} by the following relation:

$$T_{eq} = T_1 \cos^{1/4}\phi_o \qquad \text{for } 0 \leq \phi_o \leq \phi^* \text{ and } \phi^* \leq \phi \leq 2\pi$$
$$= T_2 \qquad \text{for } \phi^* \leq \phi \leq (2\pi - \phi^*) \qquad (15)$$

where T_1 is the temperature at the subsolar point taken to be 385°K, T_2 is the night-time equatorial temperature taken to be 100°K, and ϕ^* is determined in such a way that the temperature is continuous at $\phi_o = \phi^*$, i.e.

$$\phi^* = \cos^{-1}[(T_2/T_1)^4] \qquad (16)$$

For T_1 = 385°K, T_2 = 100°K, ϕ^* = 89.74° which is very close to the terminator. The idealized temperature profile is shown by dotted lines in Figure 2.

Gas Density Variations at the Surface

The density variations of gas particles at the surface are not as well known as the surface temperature variation. As mentioned in the Introduction, Hodges and Johnson (1968) showed that, by assuming the local net flux to be zero, the particle concentration and temperature at the surface satisfy $N_o T_o^{5/2}$ = constant for the case without rotation. For the surface temperature variation given by Equation (14), the concentration at the night side equator is ∿30 times that at the subsolar point. Vogel's (1966) results were in terms of molecular fluxes at the surface, from which the density may be derived. His results depend upon the prescribed steady source fluxes at the

surface, and therefore are model dependent. The most reliable way to determine the gas density at the surface is by in-situ measurements. The Apollo 14 and 15 CCGE and the Apollo 17 Lunar Surface Mass Spectrometer Experiment should provide such information. However, the data obtained from Apollo 14 so far are not sufficient to include the whole lunation. When enough data are obtained, we shall use those measurements as the basis of our calculation. Presently, for our purpose to calculate the density and flux distributions in space, we shall adopt several surface density models. The simplest one is a constant density at the surface. This is important in that the effect of lateral transport due to surface temperature variation alone can be studied. In addition, the surface density derived from models of Hodges and Johnson (1968) and of Vogel (1966) will also be used.

Computations of Density and Fluxes

By knowing the particle trajectories and the velocity distribution function at the lunar surface, the density and fluxes (and other averaged quantities) in space above the surface may be easily calculated for each species of gas. For the boundary condition of f given by Equation (12), the number density of a gas as function of position $\underline{x}$ is:

$$n(\underline{x})=\int N_o(\underline{x}_o)\left[\frac{m}{2\pi kT_o(\underline{x}_o)}\right]^{\frac{3}{2}}\exp\left[-\frac{m}{2kT_o(\underline{x}_o)}(v_r^2+v_\theta^2+v_\phi^2+2\mu\frac{r-r_o}{rr_o})\right]d^3v, \quad (17)$$

and the particle flux in the i-direction is

$$\underline{\Psi}_i(\underline{x})=\int \underline{v}_i N_o(\underline{x}_o)\left[\frac{m}{2\pi kT_o(\underline{x}_o)}\right]^{\frac{3}{2}}\exp\left[-\frac{m}{2kT_o(\underline{x}_o)}(v_r^2+v_\theta^2+v_\phi^2+2\mu\frac{r-r_o}{rr_o})\right]d^3v. \quad (18)$$

In the above equations, the delta functions in Equation (5) have been integrated out and $\underline{x}_o$ and $\underline{v}_o$ are solved from the trajectory Equations (7) - (11). The quantity $\underline{v}_o^2$ appearing in the exponential function has been expressed explicitly in terms of $\underline{v}$ and r by means of Equation (7). The quantity $\underline{x}_o$, which N_o and T_o are depending upon as functions of $\underline{v}$ and $\underline{x}$, are given by Equations (10) and (11).

Equations (17) and (18) are integrated numerically. The computational procedure is as follows. The value of the position vector $\underline{x}(r,\theta,\phi)$ at which $n(\underline{x})$ and $\underline{\Psi}_i(\underline{x})$ are to be calculated is first assigned. During the integration in velocity space, for each particular set of velocity components v_r, v_θ and v_ϕ, the values of θ_o and ϕ_o (r_o = lunar radius) are calculated by the trajectory equations (10) and (11); i.e., by tracing back along a trajectory to the position on the surface where the particle originates. Knowing the value of θ_o and ϕ_o, the surface temperature T_o is calculated according to Equations (14) and (15), and the gas density N_o is calculated by using specific surface density models. Having known the values of

T_o and N_o, the integrands of Equations (17) and (18) are then calculated and the integrations may be performed. The above numerical integrations are performed by a standard summation method. The infinite integration limits are replaced by sufficiently large finite values. The mesh size and the integration limits are varied independently until the integration converges. The program was first tested for the density $n(\underline{x})$ in the case of constant surface temperature and density, which yielded excellent agreement with the theoretical barometric formula. We then ran the program for various cases of variable surface temperature and different models of surface gas density. The results of these calculations will be discussed below.

Results and Discussion

The orbital mass-spectrometers of Apollo missions are designed to measure gases with mass number ranging from 12 to 66, and within this range neon and argon are probably the most abundant species. In the present investigation we are, therefore, primarily interested in the density and flux distributions in space for neon (20) and argon (40). As mentioned before, several models for the surface density distributions will be adopted. Here we are mainly concerned with two cases: a uniform surface density N_o throughout the entire lunar surface, and $N_o \sim T_o^{-5/2}$, i.e., the result of Hodges and Johnson. A third case for hydrogen with surface density N_o derived from Vogel

will also be investigated. All of the present calculations are normalized in such a way that $N_o = 1$ at the subsolar point.

In Figure 3, we show the density distributions of neon and argon in an equatorial orbit of 100 km height above the lunar surface for the case of uniform N_o. For this model of surface density N_o, the transport of gas particles is due to the effect of temperature variation only. As shown in Figure 3, the neon density at the subsolar point in the orbit is approximately one order of magnitude larger than that at the antisolar point; and for the case of argon, about a factor of 2.5×10^2. This is because the temperature on the dayside of the moon is much higher than that of the night side, and consequently particles emitted from the day side surface have higher energies so that the fraction of particles reaching 100 km height is larger. Most of the results shown in Figure 3 are quite close to the local scale height approximation except in the region near the terminator where the surface temperature gradient is very large and the local scale height approximation is no longer valid. But this is precisely the region of very prominent lateral transport of gas particles from the hot side of the moon to the cold side. Our results clearly show such regions of net lateral transport as the density profiles decrease gradually toward the night side. For the case of neon, this region extends to approximately 30° toward the night side beyond the terminator; and for the case of argon, about 15°.

Such net lateral transport effect may be best understood by looking at the net particle flux across the terminator. Figure 4 shows the net flux as function of height above the surface at the equatorial terminator, also for the case of uniform N_o. We observe from the results that the net flux, the difference between positive (from hot side to the cold side) and negative fluxes, across the terminator has a maximum which occurs for the case of neon at about 25 km height, and for the case of argon at 15 km. This maximum may be explained as follows. Because of the temperature contrast between lunar day and night, the distributions with height for the oppositely directed fluxes are not the same. Particles traveling from the hot side of the moon to the cold side tend to spread over a higher altitude, whereas those moving from the cold side to the hot side are restricted to lower altitudes. The difference which is the net flux turns out to have a maximum above the surface. In Figure 4, the positive flux of neon and argon is also shown (the difference between the positive flux and the net flux is the negative flux).

In Figure 5, we show the density distributions of neon and argon in an 100 km height equatorial orbit for the case of $N_o \sim T_o^{-5/2}$, i.e., the surface density distribution of Hodges and Johnson (1968). For this model, the neon density initially increases from the subsolar point with longitude ϕ, reaches a maximum approximately at the terminator, and then

decreases gradually at the night side to a value about twice that at the subsolar point. For the case of argon, the density increases form the subsolar point with ϕ, reaches a maximum approximately 20° before the terminator, and decreases rapidly at the night side to a value about one order of magnitude smaller than that at the subsolar point. It is interesting to note that, for both cases, the density variations between subsolar and antisolar points at 100 km height are not monotonic functions of ϕ, althought this is true for T_o and N_o.

The positive and negative fluxes as functions of height at the equatorial terminator, for the case of $N_o \sim T_o^{-5/2}$, are shown in Figure 6 for neon and Figure 7 for argon. Again, because of the large temperature contrast between lunar day and night, the distributions of positive and negative fluxes with height are very different, both for neon and argon. For this model of surface density N_o, the absolute values of the negative fluxes at higher altitudes are smaller than positive fluxes, but at lower altitudes, the reverse is true. The zero net flux occurs at $\sim$63 km for neon and $\sim$27 km for argon. The larger negative fluxes at lower altitudes are the result of the combination of low night-time temperatures with higher surface densities at night: lower temperatures on the night side confine most of the particles to lower altitudes, yet the larger surface density N_o on the night side ($N_o \sim T_o^{-5/2}$) provides a larger number of these particles.

The expected density variations of neon and argon as functions of ϕ for the 8 x 60 nm descent orbit of Apollo 15 are shown respectively in Figures 8 and 9 for the cases of uniform N_o and $N_o \sim T_o^{-5/2}$. The ground track and altitude elements of the 8 x 60 nm orbit are listed in Table 1, but a transformation of coordinates is made such that in our result, $\phi = 0$ is at the subsolar point. In Figure 8, which is for the case of uniform N_o, the relative change of the density at the orbit is about a factor of 50 for neon, and 3×10^3 for argon. For the case of $N_o \sim T_o^{-5/2}$, shown in Figure 9, the relative change of the density over the orbit is about a factor of 25 for neon, and 7×10^2 for argon. In this case, the density distributions, especially for neon, are peaked at both sunrise and sunset terminators.

The last case in the present investigation is the density variation of hydrogen atom at 100 km equatorial circular orbit, where the surface density N_o is derived from the flux distribution of Vogel (1966). He assumed a steady source flux proportional to the cosine of the sun angle for the sunlit side of the moon, and obtained a flux distribution at the surface. For our computations we have chosen a flux of the form $[\cos \phi_o \sin \theta_o + 0.125]$ (in arbitrary units) at the day side and a constant 0.125 at the night side. It can be shown that the surface density N_o may then be obtained from the flux distribution

by multiplying the latter by a factor $\sim T_o^{-1/2}$. After normalizing $N_o = 1$ at the subsolar point, the density distribution in 100 km equatorial orbit is shown in Figure 10. The result shows it to be very different from the local scale height approximation. For instance, at 100 km above the subsolar point, our result gives n = 0.59, the local scale height approximation would give n = 0.95. At the same height above the antisolar point, the corresponding values for density are 0.18 and 0.15 respectively. Therefore, it is clear that the atmosphere loses particles on the day side and gains particles at the night side, a process due to lateral transport. The large difference between the present result and the local scale height approximation at 100 km above the subsolar point is due to particles lost to space by the thermal escape mechanism. Therefore, the present model may also be used for the study of thermal escape in planetary exospheres, a subject which has long been of interest.

Summary and Conclusions

A theoretical model has been constructed, on the basis of the kinetic theory of gases, for the collisionless lunar atmosphere, to determine the three-dimensional spatial variations of neutral gas densities and fluxes due to non-uniform distribution of surface temperature and gas densities. The collisionless Boltzmann equation is solved by the method of characteristics, and the gas densities and fluxes are

obtained by taking moments of the velocity distribution function, which are calculated numerically. Primary emphasis is on the neon and argon density distributions in an 100 km (∿54 nm) equatorial circular orbit and an 8 x 60 nm elliptic orbit of Apollo 15, and flux distributions versus altitude across the equatorial terminator. The lunar surface temperature used for the present calculation is a good representation of the true temperature distribution. For the gas sources at the surface, two models are adopted: (1) a uniform surface density N_o, and (2) $N_o \sim T_o^{-5/2}$.

The results of density distributions, for both neon and argon, show that the relative changes in density, i.e., the ratio of maximum and minimum values, at a particular orbit may differ by orders of magnitude for different models of gas sources. The flux distributions versus altitude at the equatorial terminator for these two models of gas densities are also quite different. For the case of uniform N_o, the positive flux, which is from the hot side of the moon to the cold side, is always greater than the negative flux. However, for the case of $N_o \sim T_o^{-5/2}$, the positive flux is greater than the negative flux only above certain altitudes; below this altitude, the reverse is true. Therefore, after the Apollo orbital mass-spectrometer experiments' data are collected and analyzed, it may be possible to discriminate the various models of gas sources at the surface.

The density distribution of hydrogen atoms at the 100 km equatorial circular orbit is also calculated for a model of surface gas density derived from the flux distribution of Vogel. This model has higher surface density at the day side than that at the night side. The result shows substantial lateral transport between day and night as well as particle loss due to thermal escape. Therefore, the present model may also be used for the study of thermal escape in planetary exospheres.

Acknowledgment

The authors are grateful to Dr. P. J. Hickson for his stimulating discussions and initiation of the numerical program.

T. T. J. Yeh

T. T. J. Yeh

G. K. Chang

G. K. Chang

2015-$\frac{TTJY}{GKC}$-dmu

Attachments
Appendixes A & B
Table 1
Figures 1-10

REFERENCES

Goldstein, H., Classical Mechanics, Chapter 9, Addison-Wesley, Reading, Massachusetts, 1953.

Groves, G. V., Anticipated Vacuum Conditions on the Moon, Proceedings of the Third Lunar International Laboratory Symposium, 1967, in Research In Physics and Chemistry, Ed. F. J. Malina, Pergamon Press, New York, 1969.

Hodges, R. R., Jr., and F. S. Johnson, Lateral Transport in Planetary Exospheres, J. Geophys. Res., 73, 7307, 1968.

Johnson, F. S., Lunar Atmosphere, to be published in Rev. Geophys. Space Phys., 1971.

Johnson, F. S., D. E. Evans, and J. M. Carroll, Cold Cathode Gage Experiment (Lunar Atmosphere Detector), to be published in Preliminary Mission Science Report for Apollo 14, NASA SP publication, 1971.

NEPSAP: Natural Environment and Physical Standard for the Apollo Program and the Apollo Applications Program (M-D E 8020.008 C), NASA, Washington, D. C. 1969.

Vogel, U., Molecular Fluxes in the Lunar Atmosphere, Planet. Space Sci., 14, 1233, 1966.

APPENDIX A

EXPLICIT EXPRESSION OF THE COLLISIONLESS BOLTZMANN EQUATION AND ITS CHARACTERISTIC EQUATIONS IN SPHERICAL COORDINATES

In spherical polar coordinates (r, θ, ϕ), the collisionless Boltzmann equation is in the following form:

$$\frac{\partial f}{\partial t} + v_r \frac{\partial f}{\partial r} + \frac{v_\theta}{r} \frac{\partial f}{\partial \theta} + \frac{v_\phi}{r \sin \theta} \frac{\partial f}{\partial \phi} + \left(\frac{v_\theta^2 + v_\phi^2}{r} - \frac{\mu}{r^2} \right) \frac{\partial f}{\partial v_r} + \left(\frac{v_\phi^2}{r} \cot \theta - \frac{v_r v_\theta}{r} \right) \frac{\partial f}{\partial v_\theta} - \left(\frac{v_\theta v_\phi}{r} \cot \theta + \frac{v_r v_\phi}{r} \right) \frac{\partial f}{\partial v_\phi} = 0, \tag{A-1}$$

where v_r, v_θ and v_ϕ are the velocity components in the directions r, θ and ϕ respectively, and μ is the lunar gravitational constant.

The characteristic equations of (A-1) may be written in the following form:

$$\frac{dr}{dt} = v_r,$$

$$r \frac{d\theta}{dt} = v_\theta,$$

$$r \sin \theta \frac{d\phi}{dt} = v_\phi,$$

$$\frac{dv_r}{dt} = \frac{v_\theta^2 + v_\theta^2}{r} - \frac{\mu}{r^2} \tag{A-2}$$

$$\frac{dv_\theta}{dt} = \frac{v_\phi^2}{r} \cot \theta - \frac{v_r v_\theta}{r},$$

$$\frac{dv_\phi}{dt} = - \frac{v_\theta v_\phi}{r} \cot \theta - \frac{v_r v_\phi}{r}.$$

These are the equations of motion of a particle in spherical coordinates under the gravitational force.

APPENDIX B

DERIVATION OF PARTICLE TRAJECTORIES IN FIXED SPHERICAL COORDINATES

The Hamiltonian of a particle under a central gravitational force in a spherical coordinate may be written as

$$H = (1/2m)\ (p_r^2+p_\theta^2/r^2+p_\phi^2/r^2\ \sin^2\ \theta) - m\mu/r \qquad \text{(B-1)}$$

where μ is the Lunar gravitational constant, and p's are the momenta defined as

$$\begin{aligned} p_r &= m\dot{r}, \\ p_\theta &= mr^2\dot{\theta}. \\ p_\phi &= mr^2\ \sin^2\ \theta\ \dot{\phi}. \end{aligned} \qquad \text{(B-2)}$$

The Hamilton-Jacobi equation for the Hamilton's characteristic function w is (Goldstein, 1953)

$$\frac{1}{2m}\left[\left(\frac{\partial w}{\partial r}\right)^2 + \frac{1}{r^2}\left(\frac{\partial w}{\partial \theta}\right)^2 + \frac{1}{r^2\ \sin^2\theta}\left(\frac{\partial w}{\partial \phi}\right)^2\right] - \frac{m\mu}{r} = \alpha_1 \qquad \text{(B-3)}$$

Assuming that the solution of w is separable in the following form:

$$w = w_r(r) + w_\theta(\theta) + w_\phi(\phi), \qquad \text{(B-4)}$$

by substituting (B-4) into (B-3) the following relations may be obtained:

$$\frac{\partial w_\phi}{\partial \phi} = \alpha_\phi = \text{const.} \tag{B-5}$$

$$\left(\frac{\partial w_\theta}{\partial \theta}\right)^2 + \frac{\alpha_\phi^2}{\sin^2 \theta} = \alpha^2 = \text{const.} \tag{B-6}$$

In fact, α_1, α_ϕ and α are constants of the motion, identified as the total energy, ϕ-angular momentum and total angular momentum respectively. The solution of w may be obtained by integrating (B-5), (B-6), and (B-3), and the result is

$$w_r = \pm \int dr \sqrt{2m\,(\alpha_1 + m\mu/r) - \alpha^2/r^2},$$

$$w_\theta = \int d\theta \sqrt{\alpha^2 - \alpha_\phi^2/\sin^2 \theta}, \tag{B-7}$$

$$w_\phi = \alpha_\phi \, \phi.$$

Consider a canonical tranformation in which the new momenta P_i are all constants of the motion α_i. If the function w be denoted by $w(q_i, P_i)$, then the equations of transformation are

$$p_i = \frac{\partial w}{\partial q_i}, \quad Q_i = \frac{\partial w}{\partial P_i} = \frac{\partial w}{\partial \alpha_i} \tag{B-8}$$

According to the Hamilton-Jacobi theory, the new Hamiltonian, after the above transformation, depends on only one of the momenta α_i, and the equation of motion for $\dot{Q}$ are

$$\dot{Q}_i = \frac{\partial H}{\partial \alpha_i} = 1 \quad i = 1 \qquad \text{(B-9)}$$

$$= 0 \quad i \neq 1.$$

The immediate solutions of (B-9) are

$$Q_1 = t + \beta_1 = \frac{\partial w}{\partial \alpha_1},$$

$$Q_2 = \beta_2 = \frac{\partial w}{\partial \alpha}, \qquad \text{(B-10)}$$

$$Q_3 = \beta_3 = \frac{\partial w}{\partial \alpha_\phi},$$

where the β's are integration constants. With the solution of w given by (B-7) and (B-4), the explicit forms of (B-10) may be written as:

$$t + \beta_1 = \int \frac{m dr}{\sqrt{2m\,(\alpha_1 + m\mu/r) - \alpha^2/r^2}}$$

$$\beta_2 = \cos^{-1}\left(\frac{\cos\theta}{\sqrt{1 - \frac{\alpha_\phi^2}{\alpha^2}}}\right) \pm \cos^{-1}\left(\frac{\frac{\alpha^2}{m^2\mu}\frac{1}{r} - 1}{\sqrt{1 + \frac{2\alpha_1\alpha^2}{m^3\mu^2}}}\right) \qquad \text{(B-11)}$$

$$\beta_3 = \tan^{-1}\left(\frac{\alpha_\phi \cos\theta}{\sqrt{\alpha^2 \sin^2\theta - \alpha_\phi^2}}\right) + \phi$$

If the integration constants β's are determined in such a way that at $t = 0$, the particle leaves the lunar surface at (r_o, θ_o, ϕ_o) with velocity components $(v_{r_o}, v_{\theta_o}, v_{\phi_o})$, we obtain the particles trajectory given in the main text, Eqs. (7) - (11).

Table 1

Ground Track and Altitude Elements of the

First 8 x 60 nm Descent Orbit for Apollo 15

Latitude (Degree)	Longitude (Degree)	Altitude (nm)	Sun Angle (Degree)
25.28	.88	11.31	0
23.70	-10.07	13.82	-10
21.38	-20.70	16.93	-20
18.41	-30.97	20.56	-30
14.90	-40.89	24.62	-40
10.97	-50.50	29.00	-50
6.72	-59.91	33.58	-60
2.22	-69.33	38.28	-70
-2.75	-79.52	43.26	-80
-9.32	-93.51	49.42	-100
-13.83	-104.13	53.28	-110
-17.56	-114.23	56.15	-120
-20.71	-124.53	58.24	-130
-23.21	-135.15	59.52	-140
-24.98	-146.07	59.97	-150
-25.94	-157.21	59.54	-160
-26.04	-168.44	58.29	-170
-25.28	-179.61	56.26	180
-23.70	169.44	53.51	170
-21.37	158.80	50.15	160
-18.40	148.53	46.28	150
-14.90	138.61	42.03	140
-10.97	129.00	37.53	130
-6.72	119.59	32.91	120
-2.21	110.17	28.26	110
2.76	99.97	23.43	100
9.32	87.00	17.61	80
13.83	75.38	14.03	70
17.56	65.28	11.40	60
20.71	54.98	9.51	50
23.21	44.37	8.37	40
24.98	33.45	7.98	30
25.94	22.31	8.39	20
26.04	11.08	9.54	10
25.28	-.09	11.40	0

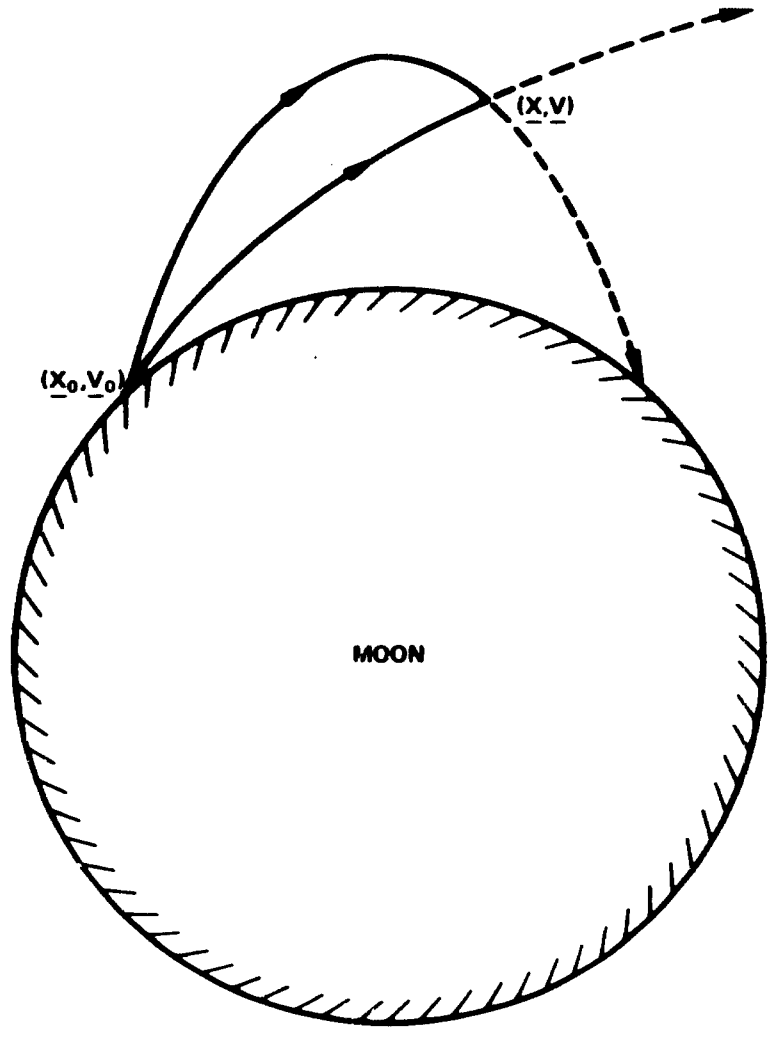

FIGURE 1 - MODEL OF PARTICLE TRAJECTORIES

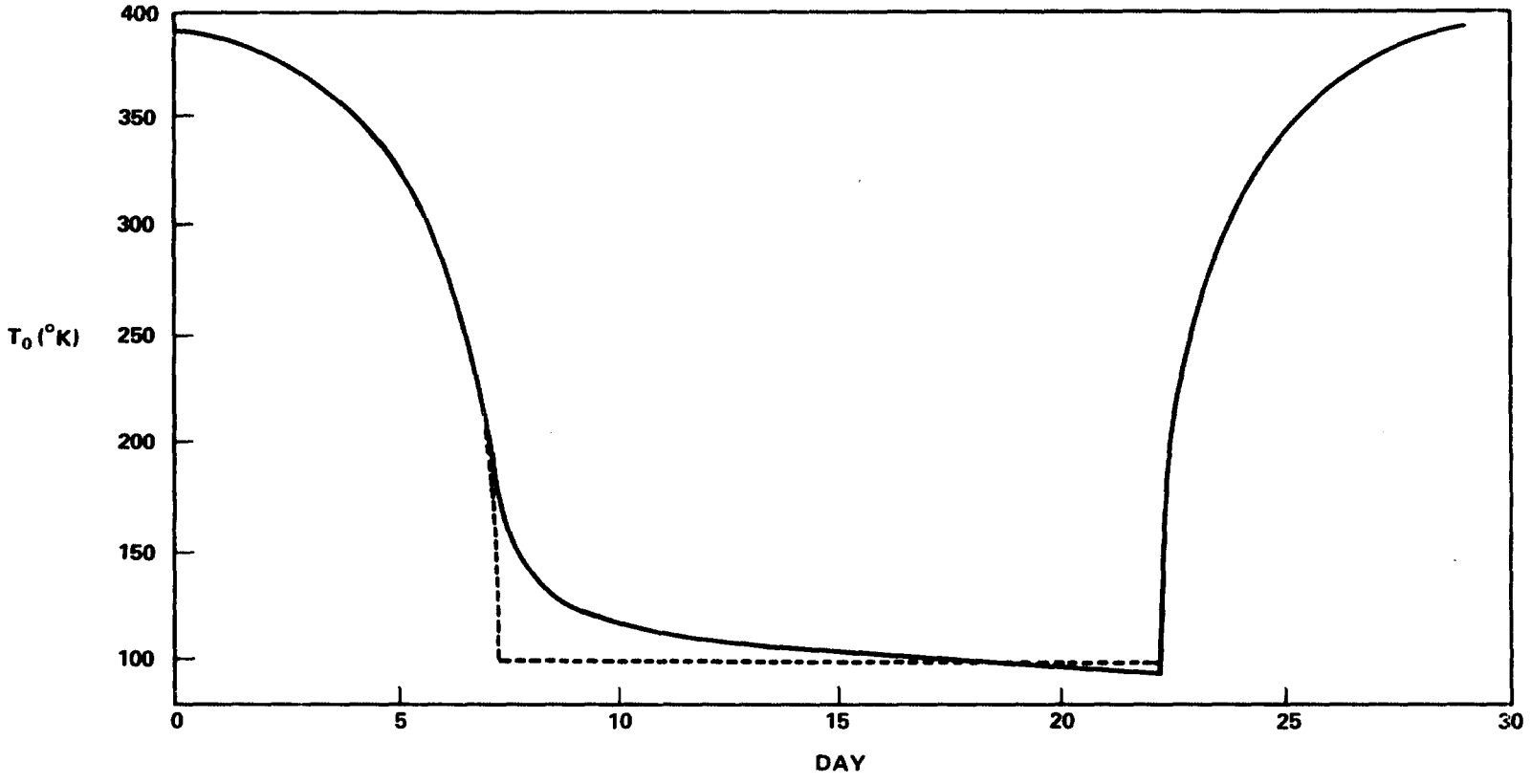

FIGURE 2 - VARIATION OF LUNAR SURFACE TEMPERATURE DURING A COMPLETE LUNATION. SOLID CURVE, GIVEN BY NEPSAP FOR THERMAL INERTIA OF 750; DOTTED CURVE, IDEALIZED.

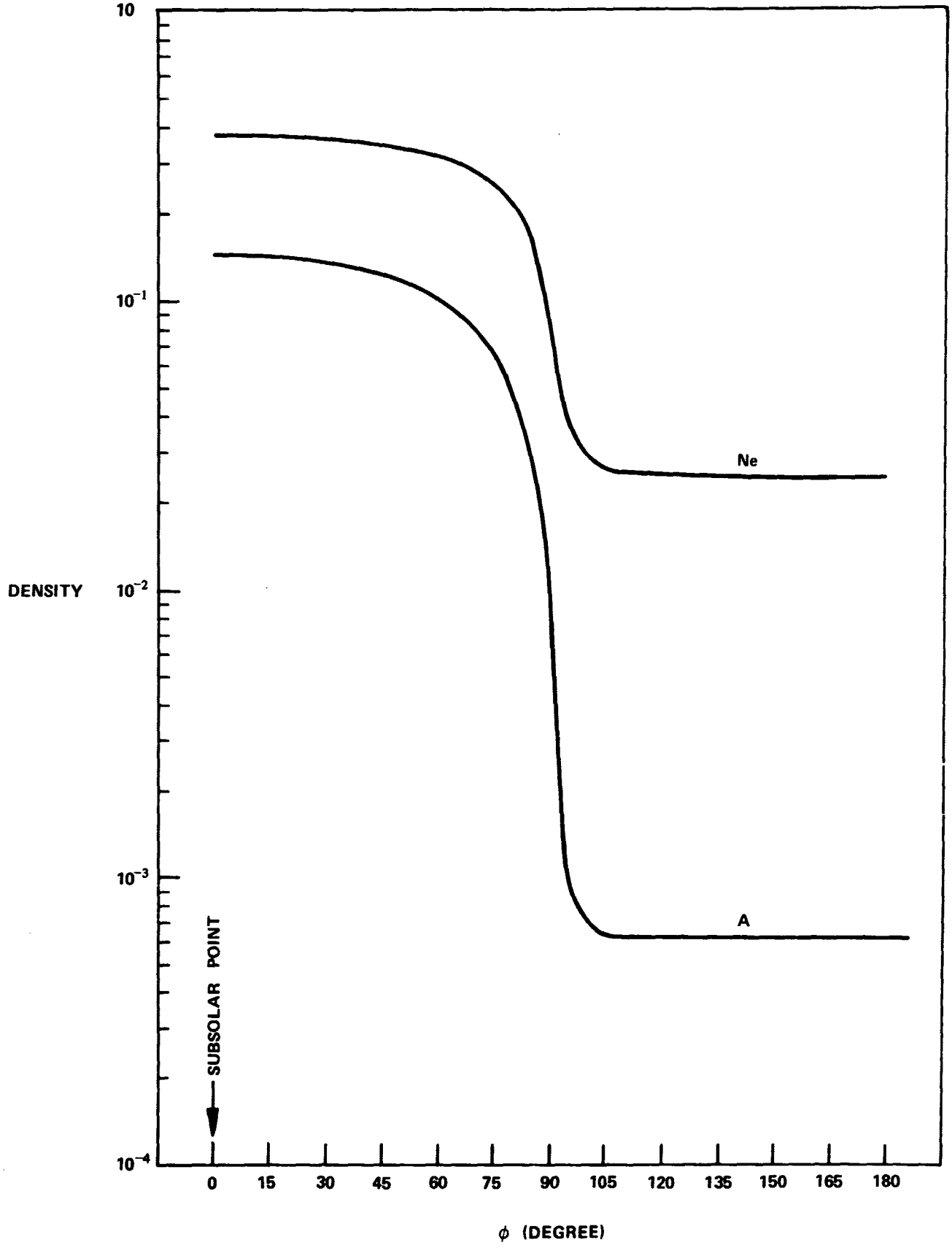

FIGURE 3 - DENSITY VARIATIONS VS ϕ IN 100 KM EQUATORIAL CIRCULAR ORBIT FOR THE CASE $N_0 = 1$

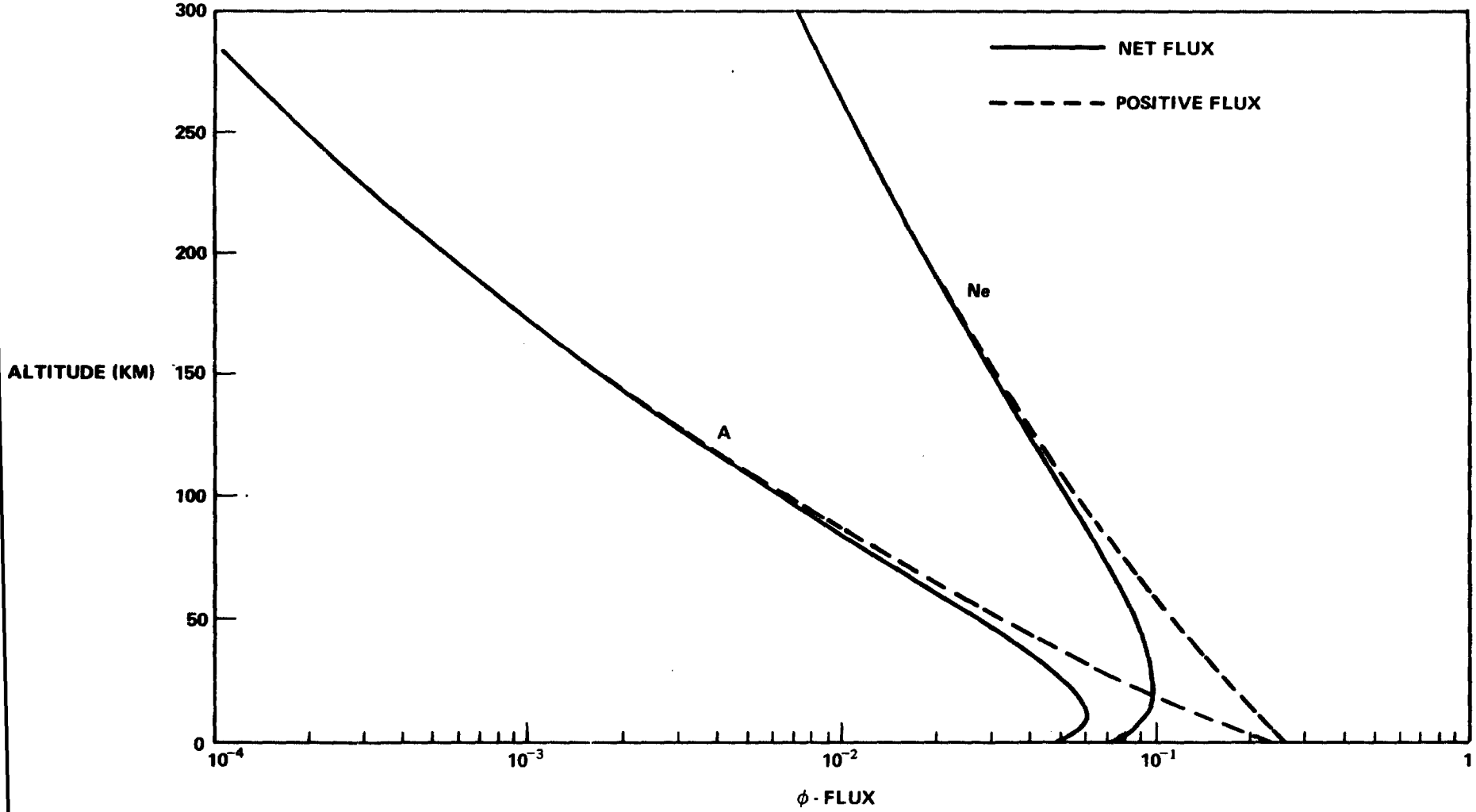

FIGURE 4 - ϕ - FLUX VARIATIONS VS ALTITUDE AT EQUATORIAL TERMINATOR FOR THE CASE OF $N_0 = 1$

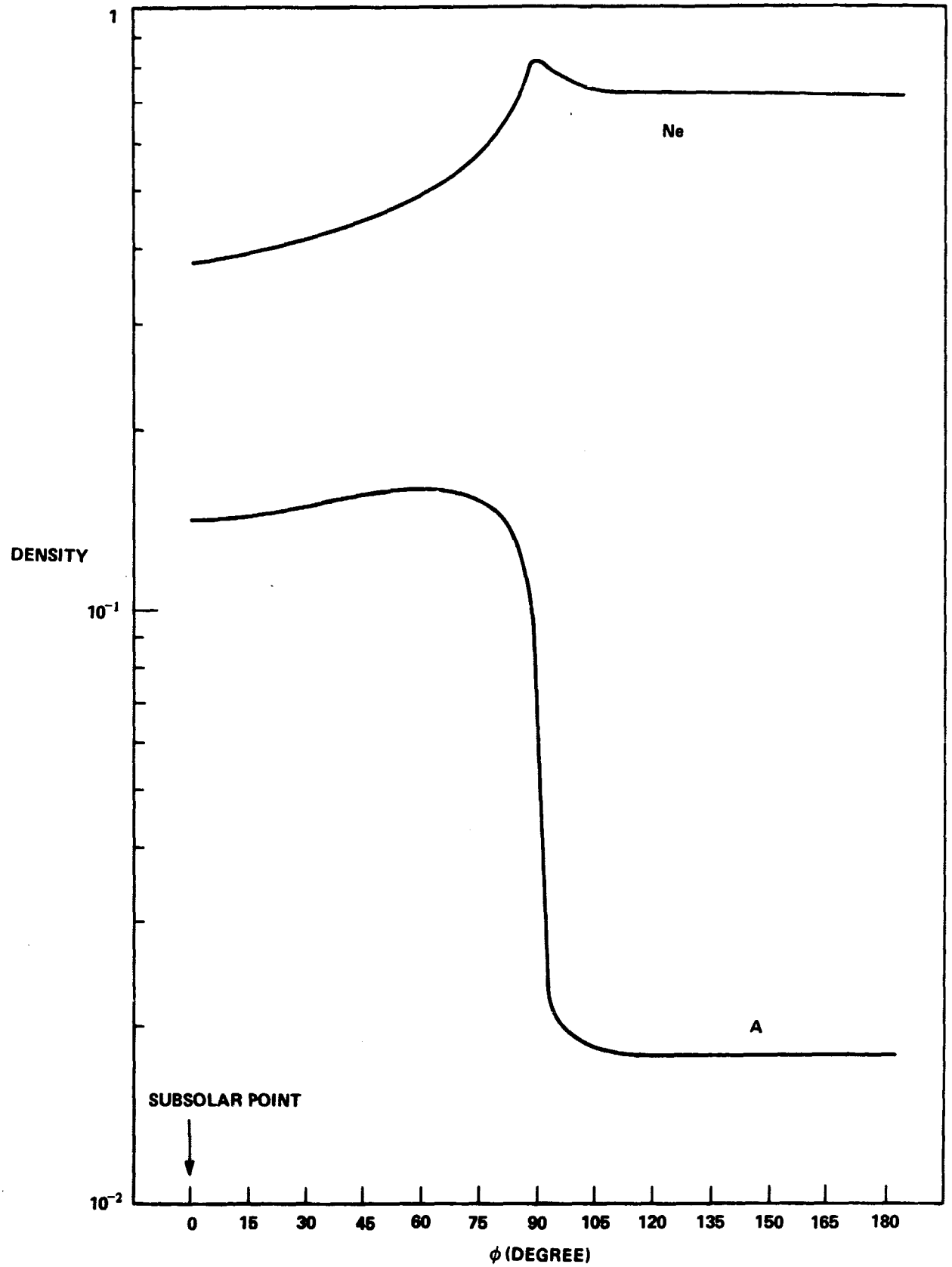

FIGURE 5 - DENSITY VARIATIONS VS ϕ AT 100 KM EQUATORIAL CIRCULAR ORBIT FOR THE CASE OF $N_0 \sim T_0^{-5/2}$

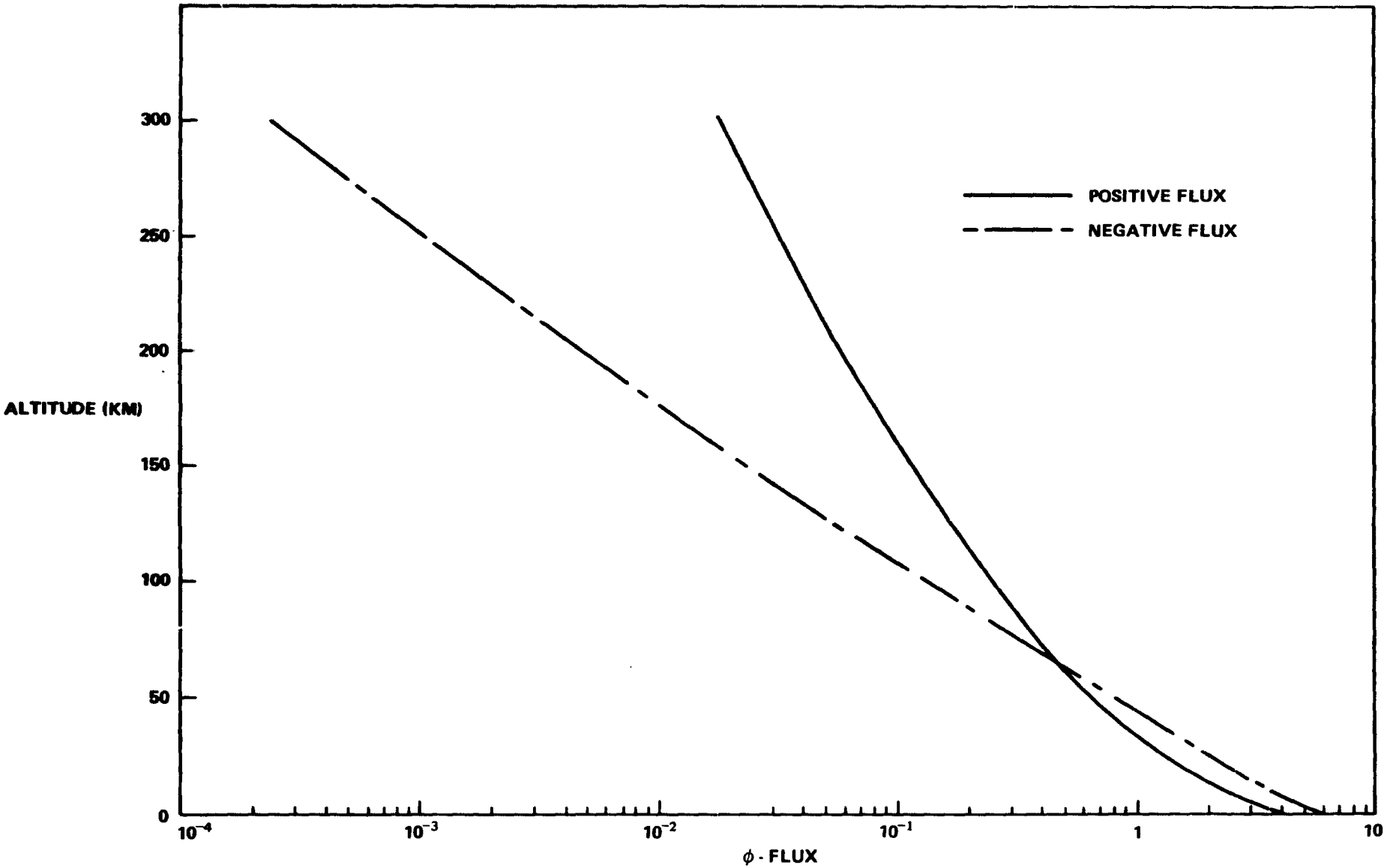

FIGURE 6 - ϕ - FLUX VARIATIONS OF NEON VS ALTITUDE AT EQUATORIAL TERMINATOR FOR THE CASE OF $N_0 \sim T_0^{-5/2}$

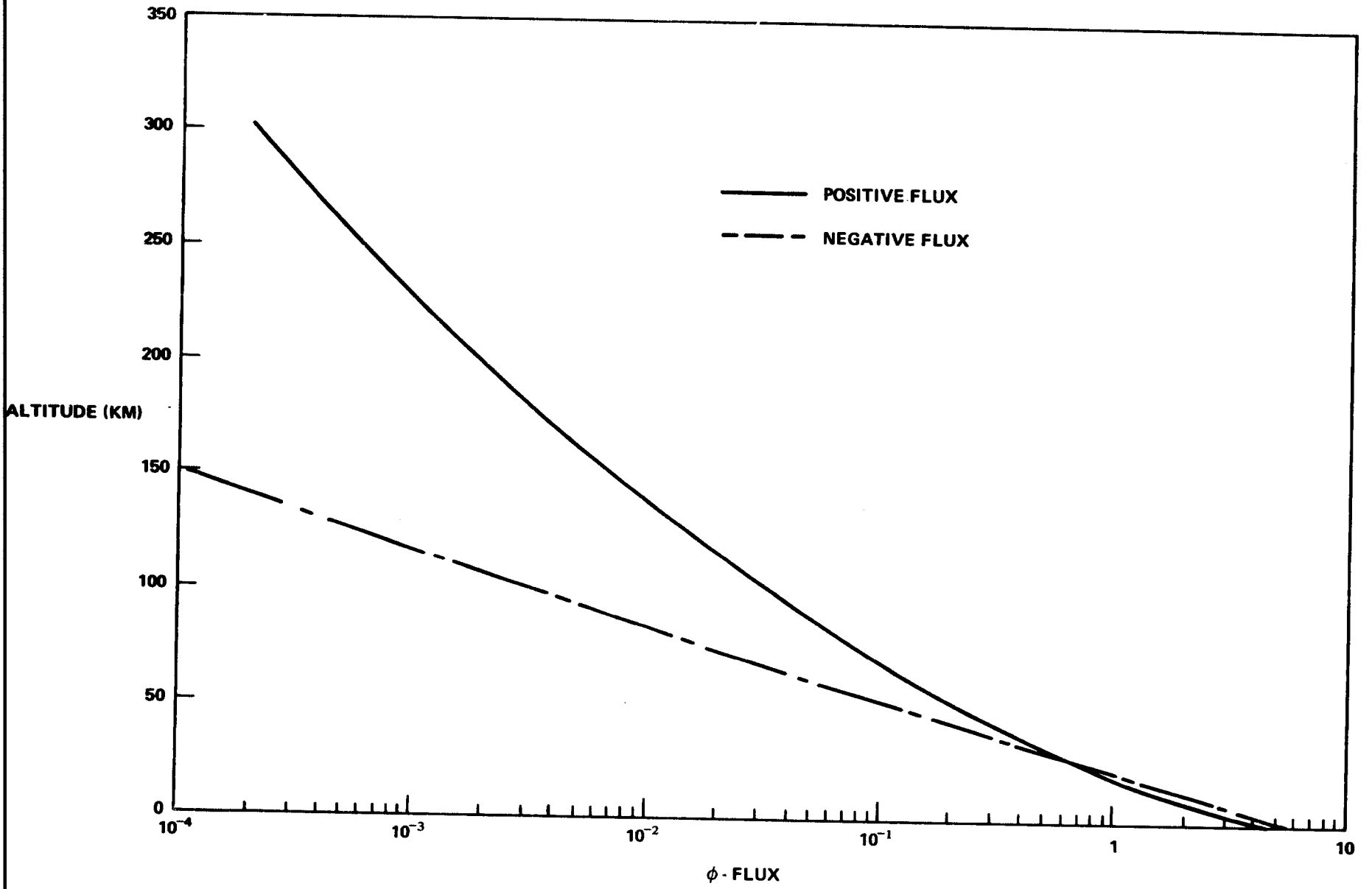

FIGURE 7 - ϕ - FLUX VARIATIONS OF ARGON VS ALTITUDE AT EQUATORIAL TERMINATOR FOR THE CASE OF $N_0 \sim T_0^{-5/2}$

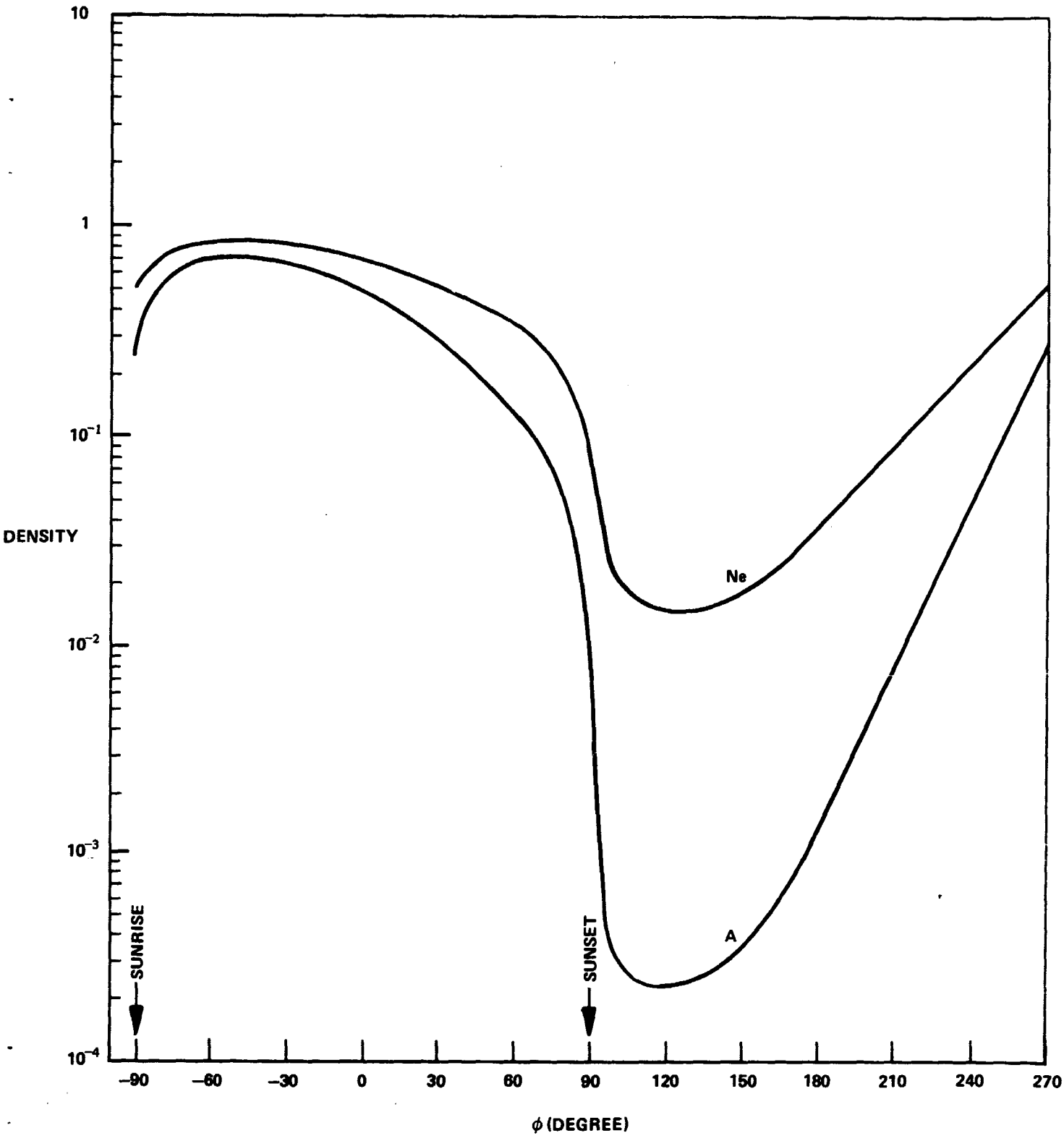

FIGURE 8 - DENSITY VARIATIONS VS ϕ AT 8 x 60 NM ORBIT OF APOLLO 15 FOR THE CASE OF $N_0 = 1$

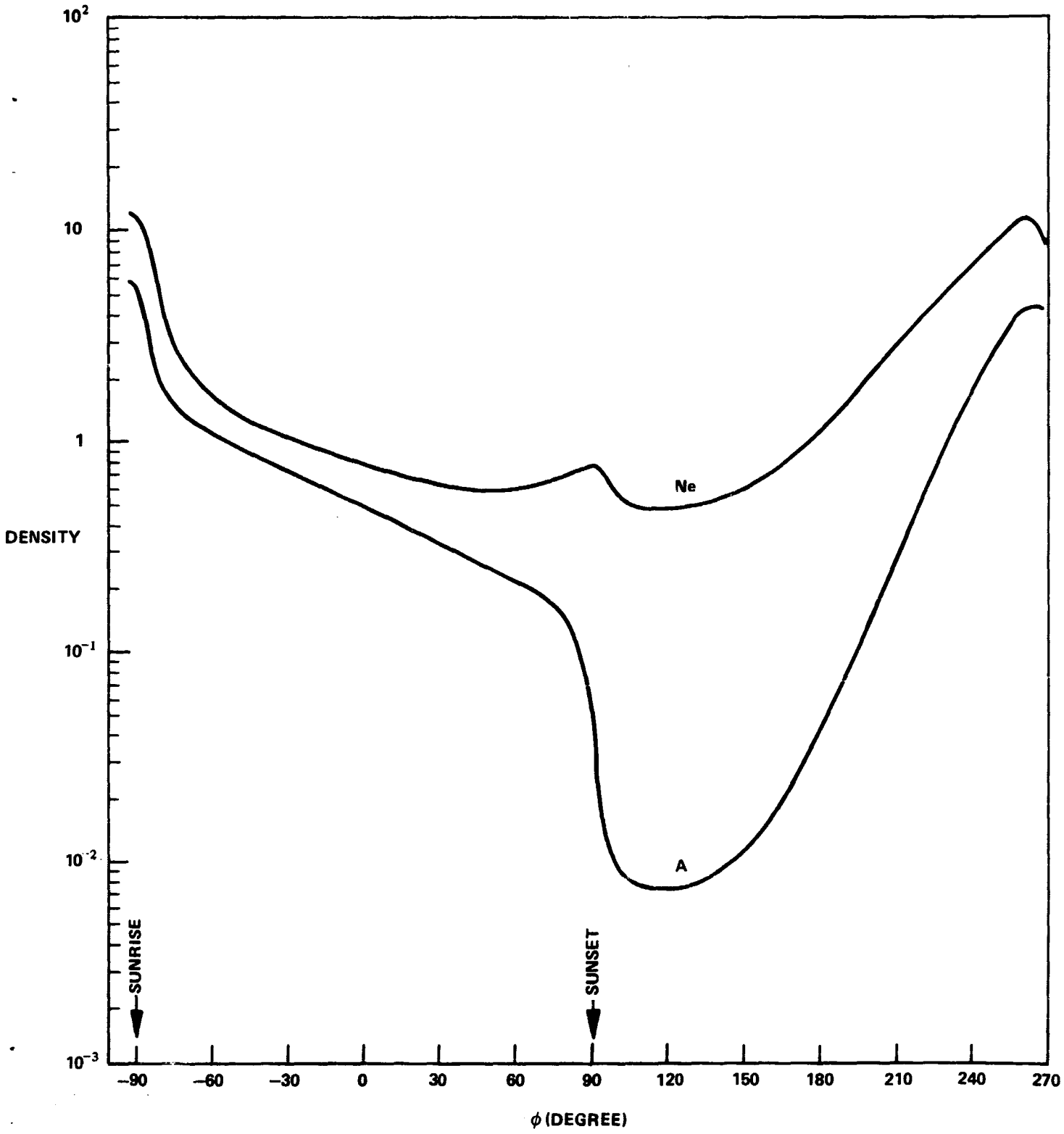

FIGURE 9 - DENSITY VARIATIONS VS ϕ AT 8 x 60 NM ORBIT OF APOLLO 15 FOR THE CASE OF $N_0 \sim T_0^{-5/2}$

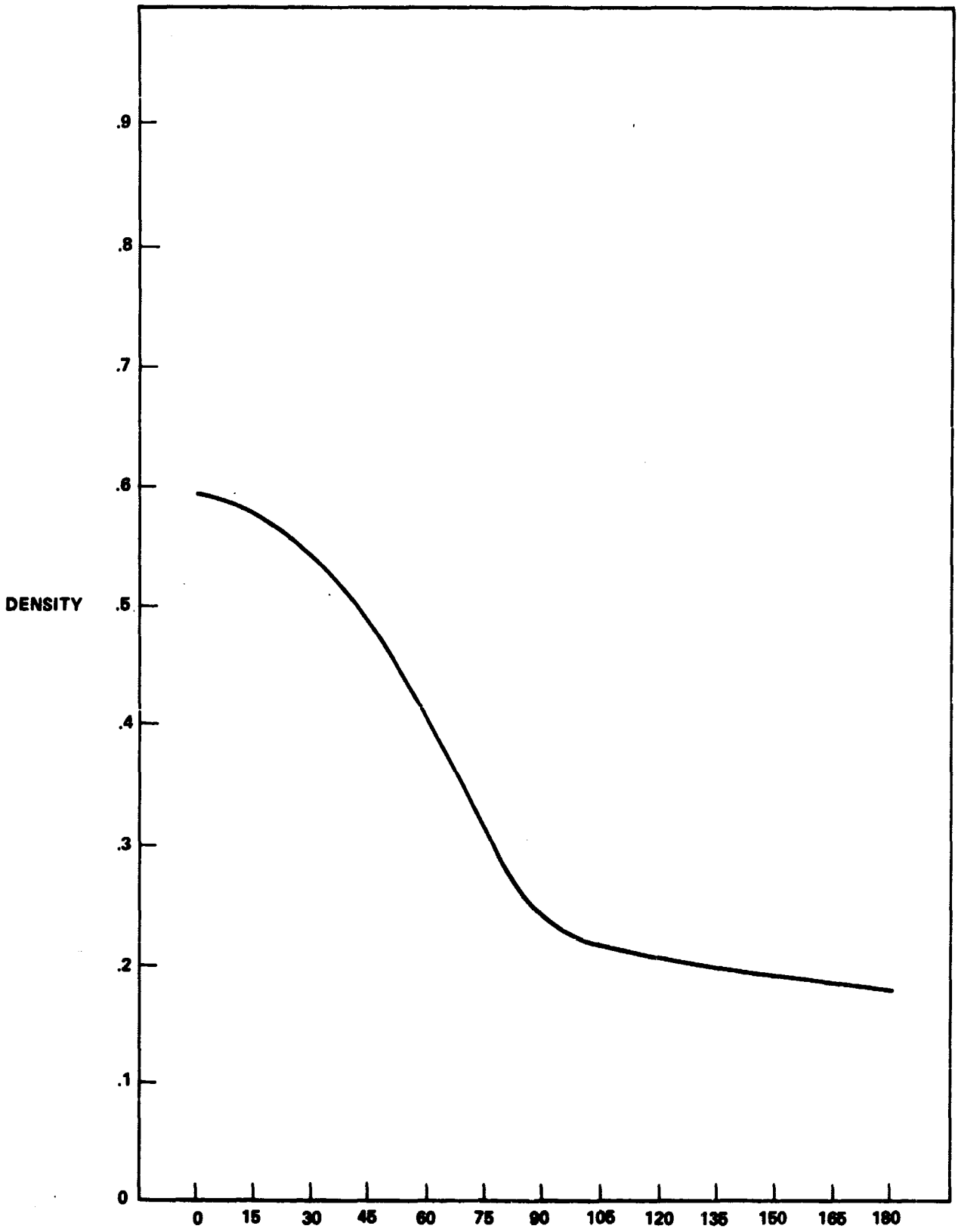

FIGURE 10 - DENSITY VARIATION OF HYDROGEN ATOMS AT 100 KM EQUATORIAL CIRCULAR ORBIT FOR THE CASE OF $N_0 \sim [\cos\phi_0 \sin\theta_0 H(90^\circ - |\phi_0|) + 0.125]\ T_0^{-1/2}$